Sensors & Actuators: A. Physical 383 (2025) 116172

Contents lists available at ScienceDirect

Sensors and Actuators: A. Physical

journal homepage: www.journals.elsevier.com/sensors-and-actuators-a-physical

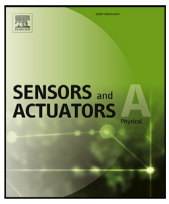

# Time-averaged interference fringe analysis: A quantitative study of nanomembrane vibration dynamics

Mengqi Fu *, Jannik Dornseiff, Valentin Barth, Elke Scheer

*Department of Physics, University of Konstanz, 78457 Konstanz, Germany*

ARTICLE INFO

*Keywords:*
Nano/micro-membrane resonators
Time-averaged interference fringes
Vibration dynamics characterization
Full-field measurement
Mode-coupling analysis

ABSTRACT

In this work, we present a method for characterizing nano/micro membrane resonators through the analysis of averaged interference fringes obtained from continuous light measurements. As the membrane vibrates, the interference fringes display blurring and contrast reduction, from which we establish a direct relationship between the vibration amplitude and the blurred area. This method offers a fast and straightforward approach to characterizing membrane vibrations and determining the dispersion relationship. Additionally, it enables the simultaneous extraction of multiple vibrational modes, providing mode numbers and phase differences that can be used to reconstruct dynamic vibration profiles. Its efficiency and broad frequency range make it particularly well-suited for high-frequency applications and rapid data collection.

## 1. Introduction

Nano/micro membrane resonators are critical components in various applications, including sensors [1,2], detectors [3], switches [4], and filtering systems [5]. They also play a significant role in fundamental research areas such as optomechanics [6], nonlinear dynamics [7,8], and other branches of physics [9,10]. Accurate characterization of the vibrational properties of these resonators is essential for optimizing their performance and understanding the underlying dynamic processes that govern their behavior. Several optical techniques, including laser Doppler vibrometry (LDV) [11,12], stroboscopic holography [13], and interferometric methods [14,15], have been widely employed for vibrational analysis due to their non-invasive nature. However, as resonators become miniaturized and the demand for high-speed, wide-bandwidth mechanical devices grows, there is an increasing need for methods that can operate over a broader frequency range, handle larger vibration amplitudes, and speed up data acquisition [3–7].

Despite their advantages, conventional optical techniques face significant limitations. LDV [12] and interferometers, such as Michelson-type interferometers [15,16], offer high temporal resolution and is ultrasensitive to small deflections, but are often restricted to single-point measurements and limited to small amplitudes. These limitations necessitate, on the one hand, scanning across the surface to obtain full-field data, which is time-consuming and may require complex control systems and, on the other hand have limited applicability to study nonlinear dynamics at large deflection amplitudes. Stroboscopic holography, while capable of capturing full-field vibrational data in a single acquisition, relies on synchronization with the excitation frequency, which can limit its application at higher frequencies and for dynamic amplitude variations [13]. These constraints highlight the need for alternative methods that can operate efficiently across wider frequency and amplitude ranges while maintaining speed and simplicity in data acquisition.

In this work, we present a method aimed at addressing these limitations by offering a direct and fast approach to characterize membrane vibrations. This method is based on the analysis of averaged interference fringes generated by continuous light measurements. As the membrane vibrates, the interference fringes exhibit blurring and contrast reduction, which we use to extract full-field vibrational data without the need for synchronized light sources or point-by-point scanning. While this approach has been applied previously to large-scale plates [17], we extend its application here to nano/micro membrane resonators, demonstrating its capability to measure in higher frequencies and resolve mode coupling phenomena at higher amplitudes. The method enables straightforward and rapid analysis over a wide frequency range and can easily handle larger vibration amplitudes. Moreover, it allows for the extraction of multiple vibrational modes simultaneously, providing mode numbers and phase differences, which can be used to reconstruct dynamic vibration profiles.

## 2. Sample fabrication and measurement method

Our experimental setup, depicted in Fig. 1(a), is built upon a suspended almost square-shaped silicon nitride (SiN) membrane framed by

* Corresponding author.
*E-mail address:* mengqi.fu@uni-konstanz.de (M. Fu).

https://doi.org/10.1016/j.sna.2024.116172
Received 31 October 2024; Received in revised form 13 December 2024; Accepted 23 December 2024
Available online 31 December 2024

a silicon (Si) chip that is attached to a piezo element. It supports flexural vibration modes labeled with mode numbers $(n, m)$, where $n$ and $m$ count the deflection extremes along the $x$- and $y$-directions. Flexural vibrations of the membranes are excited by applying an AC voltage $V_{AC}$ to the piezo. When the drive frequency $f_d$ of $V_{AC}$ approaches the membrane resonator's eigenfrequency $f_0$ of flexural modes, the membrane vibrates out of plane (denoted as $z$ axis), as shown in the insert of Fig. 1(a). To demonstrate that the surface material of the samples does not affect the method used to characterize membrane vibrations, some SiN membranes are covered with a monolayer graphene. They yield similar measurement results as the bare SiN membranes. In addition, in conventional methods like stroboscopic holography, the drive frequency signal is typically provided by a lock-in amplifier, which limits detection to the drive frequency or its harmonics. In contrast, the proposed method allows the drive frequency signal to be supplied by a standard function generator, as it does not rely on a lock-in process. This enables the detection of vibrations at all frequencies, providing a significant advantage when studying systems with complex dynamics, such as subharmonically driven or parametrically driven mechanical systems. More details of samples and experimental systems can be found in our previous work [14,18–20] and the supplementary material (SM).

To characterize the vibration properties of nanomembrane resonators, time-averaged interference patterns are obtained by using a Mirau interferometer (optical profilometer "Photomap 3D" from Fogale company) [13,19] and a digital holographic microscopy (DHM R-2100 series from the manufacturer Lyncee) [21] under continuous-light mode at room temperature. Both interferometers use a laser source with a wavelength $\lambda$ of around 640 nm.

Fig. 1(b) shows the interference fringes together with a camera view of a graphene-covered SiN membrane obtained by Mirau interferometry without mechanical excitation. The interference pattern shows parallel fringes with clear contrast and almost constant intensity along their length. The fringes are indicative of a slight inclination of the surface with respect to the normal plane of the incident light beam (along the $z'$ axis). The angle between the $z$ and $z'$ axes is very small, allowing us to approximate the in-plane coordinates as $x$ and $y$. The upper surface of the membrane is flat and almost homogeneous. Specifically, the intensity $I$ of the interference fringes depends on the reflectivity of the membrane surface and the optical path length difference between the incident and the outgoing light beams. At rest, i.e., without vibration, the $I$ at a position $M(x, y)$ on the membrane surface changes proportionally to $Z_0(x, y)$ which represents the optical path difference between the incident and outgoing beams at rest and is parallel to $z'$. We now assume (without loss of generality) that the inclination of the membrane is in $x$ direction only. This means that the interference fringes are oriented along the $y$ direction. Then, $Z_0(x, y)$ is independent of $y$ and linearly dependent on $x$ with a factor $a$: $Z_0(x) = ax$. The $I$ varies with $M(x, y)$ as:

$$I_0(x) = \frac{I_{max} - I_{min}}{2} \sin\left(\frac{4\pi Z_0(x)}{\lambda}\right) + \frac{I_{max} + I_{min}}{2}, \tag{1}$$

which match the observations in Fig. 1(b) and Fig. 2(b). Here, $I_{min}$ and $I_{max}$ are the minimal and maximal intensity of the fringes, respectively.

When a $V_{AC}$ of 100 mV ($f_d$ = 255.92 kHz) is applied to the piezo element, a flexural mode is excited to vibrate with a vibration amplitude of around 300 nm (determined by the stroboscopic light measurement shown in the SM). The flexural modes of membranes can be labeled with mode numbers $(n, m)$, where $n$ and $m$ count the deflection extremes along two sides of membranes. According to the stroboscopic light measurement, only one deflection extreme is found cross the whole membrane and in the center of the membrane, and therefore the excited flexural mode is the (1,1) mode, i.e., the fundamental mode. As depicted in Fig. 1(c), under continuous-light measurement, the time-averaged interference fringes in the two ring regions blur and the contrast of the fringes in other parts of the membrane is reduced, especially in the center of the membrane.

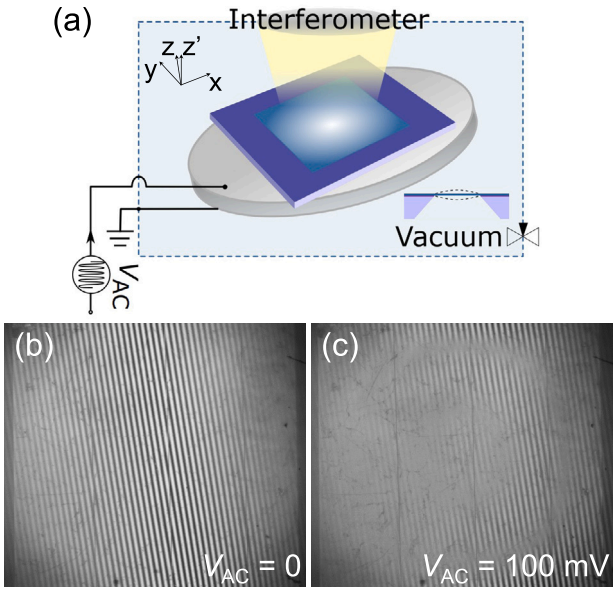


**Fig. 1.** (a) Schematic drawing of a suspended membrane resonator and the measurement scheme. The experiment employs a Cartesian coordinate system, where the $x$ and $y$ axes lie in the plane of the nanomembrane, and the $z$ axis is perpendicular to that plane and represents the out-of-plane vibration displacement. The incident laser beam (along the $z'$ axis) is slightly inclined with respect to $z$, introducing a very small angular deviation that accounts for the optical path difference. The origin $(0, 0)$ is defined as the bottom-left corner of the membrane, and the $x$ and $y$ axes are aligned with its edges. The interference fringe patterns are recorded in this coordinate system, where the spatial coordinates $(x, y)$ correspond to positions on the membrane. (b) and (c) are the camera views and interference pattern on a membrane without and with vibration amplitude of 300 nm under continuous-light mode, respectively. The membrane is a SiN membrane covered with one monolayer of graphene. The thickness of the SiN membrane is around 110 nm and its lateral size is 494 μm × 499 μm. All measurements were performed in a vacuum chamber at pressure $p \leq 0.01$ mbar and at room temperature.

This reduction in contrast can be implemented as an indicator of the vibration amplitude and pattern [17]. For the case of a membrane surface vibrating out of plane, each position $M$ has a time dependent displacement $A(x, y, t)$ with respect to $Z_0$, and its position along the $z'$ axis at time $t$ is given approximately by $Z(x, y, t) = Z_0(x) + A(x, y, t)$. The intensity at position $M$ varies with time $t$ as:

$$I(x, y, t) = \frac{I_{max} - I_{min}}{2} \sin\left(\frac{4\pi Z(x, y, t)}{\lambda}\right) + \frac{I_{max} + I_{min}}{2} \tag{2}$$

In a continuous-light measurement, the obtained interference pattern is time-averaged. Therefore, the time-averaged intensity $I_{ave}(x, y)$ is an integral over $A(x, y, t)$ and time $t$ for each $M(x, y)$:

$$\begin{aligned} I_{ave}(x, y) &= \frac{1}{\Delta t} \int_0^{\Delta t} I(x, y, t)\, dt \\ &= \frac{1}{\Delta t} \int_0^{\Delta t} \left( \frac{I_{max} - I_{min}}{2} \sin\left(\frac{4\pi Z(x, y, t)}{\lambda}\right) + \frac{I_{max} + I_{min}}{2} \right) dt \end{aligned} \tag{3}$$

When the vibration amplitude of $A(x, y, t)$ is large enough, $I(t)$ oscillates between $I_{max}$ and $I_{min}$ and thus the difference of $I_{ave}$ among different $M$ becomes smaller, leading to the loss of contrast of the interference fringes as well as to the blurring at some parts of the vibrating membranes.

## 3. Characterization of the vibration of single flexural mode

When only one flexural mode is excited in the membrane resonator, each position $M$ vibrates harmonically around $Z_0$ with the circular frequency $\omega$ with an amplitude of $A_0(x, y)$, and the $Z(x, y, t)$ is:

$$Z(x, y, t) = Z_0(x) + A_0(x, y) \sin(\omega t) \tag{4}$$

, as shown in Fig. 2(a). For the position $M$ with the lowest $I_0$ (marked by a purple dot as position I in Fig. 2 (b–d)), $I_{ave}$ becomes close to $\frac{I_{max}+I_{min}}{2}$, when $A_0$ is around 123 nm (labeled as $A_1$ in Fig. 2(c) and (d)). For position $M$ with $I_0 = \frac{I_{max}+I_{min}}{2}$ (marked by a red dot as position II in Fig. 2 (b–d)), its $I_{ave}$ keeps the same value for different $A_0$, because the intensity changes symmetrically w.r.t position II. Consequently, the averaged intensity difference between positions I and II disappears and the interference fringes blur as shown in Fig. 2(d). Note that the threshold amplitude $A_0$ for the onset of the first blurring is strongly dependent on the laser wavelength, with its value slightly smaller than $\lambda/5$.

As $A_0$ increases further to a value of around 190 nm (referred to as $A_2$ in Fig. 2), $I_{max}$ turns to relatively high intensity in position I. Therefore, position I changes from dark to bright in the obtained time-averaged pattern, as shown in Fig. 2(d). Since $I_{max}$ oscillates with the increase of $A_0$ for $M$ except at position II, the bright and dark fringes in the time-averaged pattern also alternate with reducing contrast upon increasing $A_0$. Therefore, the blurring regions as shown in Fig. 1(c) and Fig. 2(d) as well as in our previous work [15] can be considered as contour lines for the vibration amplitude $A_0$. When this feature is implemented with the vibration properties of the nanomembrane, the time-averaged interference fringes can be used as tool to characterize the vibration patterns and thus the mode numbers of the flexural modes.

Fig. 3(a)–(c) show the time-averaged interference pattern obtained from the camera view, the extracted phase diagram and the contrast image when the membrane vibrates in the (1,1) mode with a maximal vibration amplitude of around 300 nm. The time-averaged interference fringes, contrast image, and phase diagram in Fig. 3 (d–f) were calculated based on the vibration profile of (1,1) flexural mode of the square-shaped membrane resonator. The calculation integrates the instantaneous interference intensity over one vibration period. The out-of-plane displacement was simulated using a sinusoidal vibration profile for the (1,1) mode, and MATLAB was used to compute the time-averaged intensity and contrast maps. Detailed equations and parameters used in the simulation are provided in the SM. The calculated images match well with the experimental results, which confirms that the vibration amplitude of the nanomembrane can be estimated by the time-averaged interference fringes easily and quickly. In addition, this method allows for extending the frequency range to an unlimited upper end. It offers a distinct advantage over other characterization methods such as the stroboscopic light measurement which is limited by the switching time of the stroboscopic light source. These advantages benefit the measurements requiring substantial time and/or broad frequency ranges. For instance, Fig. 4 shows the application of time-averaged interference fringes in characterizing the dispersion relationship of a graphene-covered SiN membrane. The eigenfrequencies of various flexural modes, labeled $f_{0i}$ for mode $i$, are efficiently estimated by extracting the $f_{di}$ value when a blurring of the time-averaged interference fringes occurs in the positions with high absolute deflection. The estimated $f_{0i}$ values (blue dots in Fig. 4) exhibit a linear relationship with the wavelength $1/\lambda_m$ of the respective flexural mode. They are consistent with those obtained from measuring the frequency response curves of the flexural modes using vibrometry (purple stars in Fig. 4). This linear relationship aligns with previous studies on thin nanomembranes with relatively high prestress [19,20]. In such membranes, the frequency dispersion is primarily dominated by the stress within the membrane, while the effect of the bending stiffness is negligible. For the given membrane here, the slope of the fitted line is 28.91 ± 0.32 kHz· mm which is very close to the fitted value 28.87 ± 0.21 kHz· mm obtained by determining $f_{0i}$ from the frequency response curves acquired by vibrometry measurements [18].

The time-averaged interference fringes provide a fast and efficient method for determining the eigenfrequencies of nanomechanical resonators. The acquisition time depends on the vibration frequency and the camera's refreshing rate, which in our setup is typically in the order of milliseconds. The processing time is minimal, as it involves simply detecting the blurring of interference fringes and recording the corresponding drive excitation frequency. This process allows the drive frequency sweep rate to be set at the maximum refreshing speed of the camera, enabling rapid acquisition. In comparison, vibrometry measurements (as shown in Fig. 4) require recording a full frequency response curve, which typically takes several minutes or longer. Another widely used method, stroboscopic holography, measures vibration profiles by capturing quasi-static images at multiple phases of

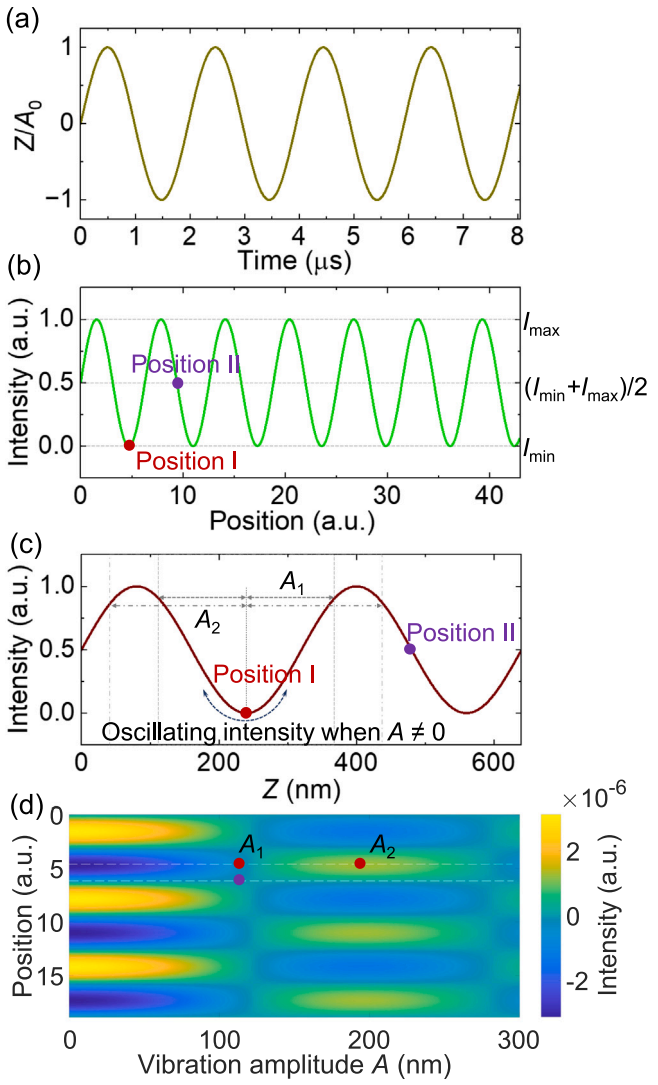


**Fig. 2.** (a) illustrates the relationship between the time dependent position $Z(t)$ along the $z$-axis at time $t$, with the vibration frequency set to 500 kHz. (b) Dependence of the intensity of the interference fringes on the position of a homogeneous flat plane. The red dot (labeled as position I) lies within the destructive interference region, while the purple dot (labeled as position II) is positioned in the transition region between constructive and destructive interference. (c) Dependence of the time-dependent intensity of the interference fringes at position $Z$. At position I, the intensity periodically varies as time progresses. When a single flexural mode is excited, $Z$ follows the trajectory shown in panel (a) as a function of time. The dotted and dash-dotted lines denote the range that position I reaches under vibration amplitudes $A_1$ and $A_2$, respectively. (d) Development of the interference contrast distribution with vibration amplitude $A$ obtained by integrating $I(t)$ over time for different positions on the flat plane. When the vibration amplitude is $A_1$, the contrast between constructive and destructive areas is small and thus a blurring occurs. As the vibration amplitude further increases, the areas of constructive interference turn to destructive interference and vice versa. (For interpretation of the references to color in this figure legend, the reader is referred to the web version of this article.)

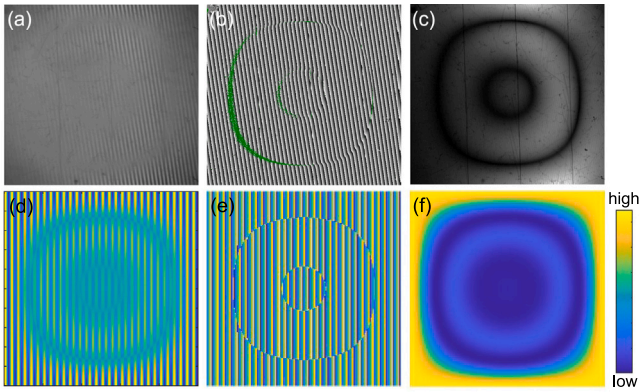


**Fig. 3.** (a) The interference fringes under camera view. The $V_{AC}$ = 100 mV and $f_d$ = 255.92 kHz. (b) and (c) are the extracted phase diagram and contrast image from panel (a), respectively. (d–f) are the calculated interference fringes, phase diagram and contrast image when the (1,1) mode is excited to $A_0$ = 300 nm.

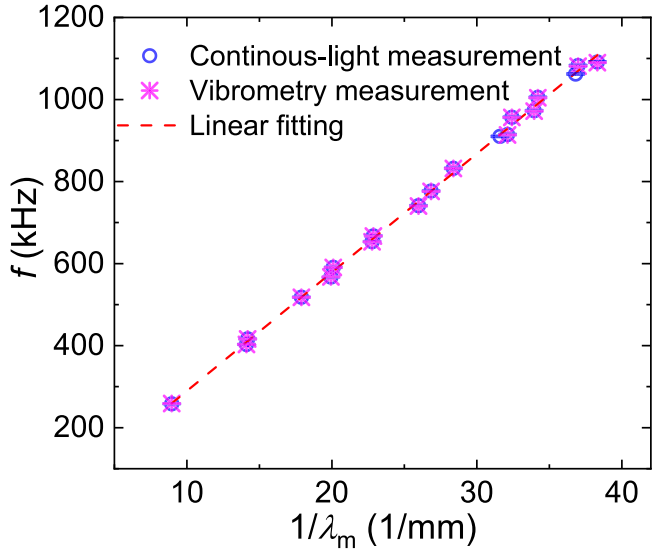


**Fig. 4.** The dispersion relation of the graphene-covered SiN membrane resonator. The eigenfrequencies are characterized by observing the appearance of the blurring area in the time-averaged images of the interference fringes in continuous-light measurement (blue circles) and by measuring the frequency response curves (purple asterisks). The standard deviations of $f_{0i}$ obtained from the two measurement methods are primarily influenced by a temperature-induced frequency drift and the measurement procedures. For the continuous light measurement, the uncertainty is estimated to be less than 0.1%. The vibrometry measurement provides higher accuracy but is more susceptible to temperature fluctuations because of the longer acquisition times. The detailed measurement methods and analysis of the standard deviation can be found in the SM. (For interpretation of the references to color in this figure legend, the reader is referred to the web version of this article.)

the vibration. To achieve sufficient contrast, each phase requires averaging over several tens of vibration periods. In practice, obtaining vibration profiles at a single drive frequency with stroboscopic holography typically requires several hundreds of milliseconds to several minutes. By contrast, the time-averaged interference fringe method provides a real-time and significantly faster alternative for identifying the eigenfrequencies.

## 4. Characterization of the vibration in mode-coupling regime

The averaged interference fringes are also able to provide the vibration information when more than one flexural mode vibrates simultaneously. In Fig. 5, the fundamental mode (1,1) mode of a SiN membrane is driven by a strong excitation $V_{AC}$ = 1 V from off-resonance below its linear eigenfrequency to high-amplitude states above it. Panel (a) and (b) are the frequency response curves in the center and quarter part of a SiN membrane (as marked in the images) measured by the stroboscopic light mode of the interferometer (DHM R-2100, Lyncee). When the drive frequency $f_d$ is between 370 to 376.1 kHz, a shark-fin shaped response is also observed for the second harmonic of $f_d$ ($2f$) in panel (b) and for the third harmonic of $f_d$ ($3f_d$), which indicates that the flexural modes with eigenfrequencies close to $2f$ and $3f_d$ are coupled into the vibration sequentially. The downward jumps observed in Fig. 5(a) and (b) occur at the harmonics ($2f$ and $3f$) of the drive frequency, where the coupled flexural modes decouple from the vibration. This behavior is validated by both the nanomembrane profiles obtained through stroboscopic light measurements and the time-averaged interference fringes. In contrast, the $1f$ response corresponds to the vibration amplitude of the (1,1) mode in the selected area and remains in a high-amplitude state, even after the responses at $2f$ and $3f$ show downward jumps. The eigenfrequency of the (1,1) mode can still be approximately identified within the range of the drive frequency where the $1f$ vibration amplitude begins to increase significantly, despite the presence of the mode-coupling effects.

Besides, the spiky shape of the $1f$ response is reflected by peaks in the third harmonic of $f_d$ ($3f$), demonstrating that other flexural modes are excited additionally. These signals are much more pronounced in the quarter position (panel (b)) than in the center of the membrane (panel (a)). The sharp peaks in the frequency response curves are attributed to the presence of vibration amplitudes at frequencies that differ from the drive frequency or its harmonics. In stroboscopic light measurements, holographic acquisition for a single phase of the vibration period is repeated multiple times to achieve an adequate signal-to-noise ratio. When the vibration frequency coincides with the drive frequency or its harmonics, the membrane profile remains consistent across repeated acquisitions. Consequently, the integral holography captures the membrane's profile accurately for that phase. However, when a vibration frequency component is present outside the drive frequency or its harmonics, the repeated acquisitions yield inconsistent holograms. These inconsistencies result in a time-averaged effect during the stroboscopic light measurement, where the acquired hologram does not represent a single vibration phase accurately. This imperfection introduces an error during data post-processing, manifesting itself as sharp peaks or dips in the frequency response curves.

Traditionally, a series of quasi-static profiles of the membrane measured under different phases in one vibration period or a ring-down measurement are necessary to determine which flexural modes are coupled in the mechanical system. In this work, we demonstrate that the mode numbers as well as the phase difference between the coupled flexural modes can be quickly estimated by the measurements of time-averaged interference fringes. Fig. 5 (c-h) demonstrate the contrast images of time-average measurements on the whole membrane with increasing $f_d$. The $V_{AC}$ = 1 V and the $f_d$ is 371.6, 372.4, 373.2, 373.8, 375.7 and 376.0 kHz for panel (c-h), respectively. From Fig. 5(c) and (d), we observe that the contrast images deviate from the ring shape and an additional diagonal feature appeals, indicating that the (2,2) mode is coupled into the vibration. By doing the simulation for various phase differences between the (1,1) and (2,2) mode as shown in Fig. 6 and Fig. S3 in the SM, we show that the difference on the patterns in Fig. 5(c) and (d) are not only due to the slight amplitude difference but also the phase difference between the two vibrating flexural modes. By using the mode numbers and phase differences, the dynamic vibration profiles can be reconstructed, for instance, in MATLAB, as shown in the SM.

The mode numbers and phase differences between coupled flexural modes in a nanomembrane mechanical resonator are critical for understanding and controlling the system's vibrational behavior. The mode numbers provide key information about the spatial mode shapes,

the frequency-mode number relationship, and the mechanisms of mode coupling [22–24]. The phase difference between these modes further governs how they interact, determining whether they interfere constructively or destructively understanding these parameters enables precise tuning of coupled modes, allowing for improved stability, reduced energy dissipation, and enhanced control in applications requiring fine-tuned vibrational states [22,24–26].

The pattern keeps varied at different detunings. As shown in Fig. 5(f) and (g), with a high response appearing in $3f$, the vibration pattern of (3,3) mode is added into the observed contrast images, indicating that not only (2,2) mode but also (3,3) mode have been coupled into vibration. Once the responses at $2f$ and $3f$ drop, the contrast image reverts to a ring-shaped pattern, as shown in Fig. 5(h).

Moreover, time-averaged interference fringes cannot only be used to characterize the vibration properties of a nanomembrane, but can also be combined with other measurement techniques, such as stroboscopic light measurements. For instance, by observing contrast images during stroboscopic illumination, one can quickly and easily determine if any flexural modes are vibrating at other frequencies or if the nanomembrane is in a chaotic state. Using the time-averaged interference fringes as a complementary approach enhances the overall measurement efficiency and provides additional information on vibrations in the nonlinear regime. However, care has to be taken when determining absolute deflection amplitudes from the time-averaged data, since the interference fringes may lead to a systematic underestimation of the actual amplitudes while correctly reproducing the mode shapes [23]. In addition, the proposed method can be applied to MEMS resonators with various geometries or complex structures, provided that interference fringes can be captured with sufficient contrast and sufficiently small uncertainties. One aspect that may require further consideration is the potential variation in material or surface reflectivity, which could influence the contrast and quality of the interference fringes. To mitigate this risk, interference fringes of the structure in a static, non-vibrating state can be initially recorded to calibrate surface reflectivity and material properties. This approach enhances the robustness of the method when applied to structures with heterogeneous surfaces or unconventional designs.

## 5. Conclusion

In this work, we demonstrate a method for characterize nano/micro membrane resonators by analyzing averaged interference fringes obtained from continuous light measurements. The technique effectively establishes a direct relationship between the vibration amplitude and the blurring of the interference fringes, providing a simple and efficient approach to characterizing membrane vibrations without frequency limitations. We also present that the developed method is particularly advantageous for rapid data acquisition by measuring the dispersion relationship of the membrane resonator, as it allows for full-field measurements without the need for synchronized light sources or point-by-point scanning. Additionally, it enables the extraction of information on multiple vibrational modes in the mode coupling regime, including mode numbers and phase differences, which can be used to reconstruct dynamic vibration profiles. This capability offers a comprehensive understanding of complex vibrational behaviors. As a side remark, the nonlinear optical transduction phenomena occurring in the time-averaged data used in this work, may also result in misinterpretation of the interference patterns [15]. Therefore a careful comparison with either stroboscopic data acquisition or non-optical methods [8] is necessary to separate artifacts from real mode shapes. Overall, the presented method is well-suited for applications requiring fast and broad-frequency-range characterization of membrane resonators. Its ability to capture both high-frequency vibrations and complex mode coupling phenomena makes it a valuable tool for advancing the study of nano/micro-scale mechanical systems.

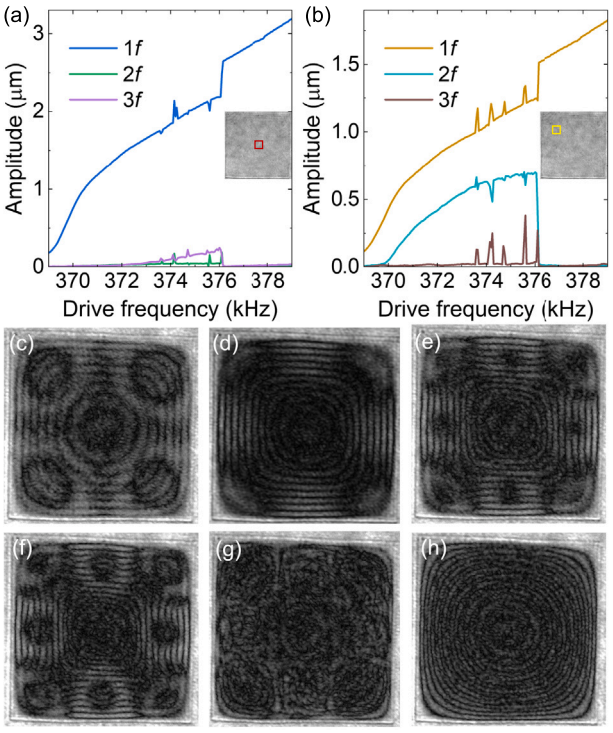


**Fig. 5.** (a) and (b) are the frequency response curves of a SiN membrane resonator measured in the center and quarter of the membrane, respectively. The thickness of the SiN membrane is around 300 nm and the side length around 570 μm. The measurements are performed in the stroboscopic light mode for $V_{AC}$ = 1 V. The insets show the contrast images of the SiN membrane without drive power. The measurement points are marked by squares. (c)–(h) are the contrast images of time-average measurements on the whole membrane at $V_{AC}$ = 1 V. The drive frequency is 371.6, 372.4, 373.2, 373.8, 375.7 and 376.0 kHz, respectively.

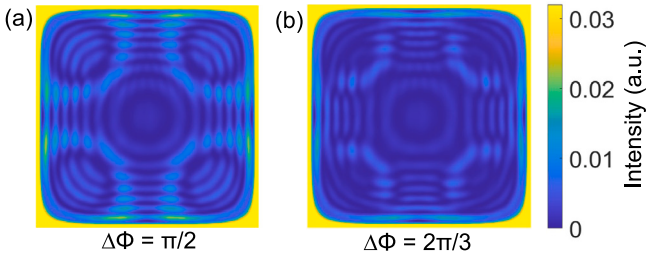


**Fig. 6.** (a) and (b) show the calculated contrast images when (1,1) and (2,2) modes are excited simultaneously and have phase differences of $\pi/2$ and $2\pi/3$, respectively. The vibration amplitudes of (1,1) and (2,2) modes are set as 1300 and 450 nm, respectively.

## CRediT authorship contribution statement

**Mengqi Fu:** Writing – review & editing, Writing – original draft, Visualization, Validation, Methodology, Investigation, Formal analysis, Data curation, Conceptualization. **Jannik Dornseiff:** Methodology, Investigation. **Valentin Barth:** Writing – review & editing, Investigation. **Elke Scheer:** Writing – review & editing, Visualization, Validation, Supervision, Resources, Project administration, Methodology, Investigation, Funding acquisition, Formal analysis, Data curation.

## Declaration of competing interest

The authors declare that they have no known competing financial interests or personal relationships that could have appeared to influence the work reported in this paper.

## Acknowledgments

The authors thank L. Catalini, J. Boneberg and F. Yang for fruitful discussion and comments about the work. The authors acknowledge the use of the experimental equipment and the expert support concerning its usage and data analysis provided by the Nanostructure Laboratory at the University of Konstanz. The authors gratefully acknowledge financial support from the A. v. Humboldt Foundation and the Deutsche Forschungsgemeinschaft (DFG, German Research Foundation) through SFB 1432 (Project-ID 425217212) and Project IDs 449653034 and 510766045.

## Data availability

Data will be made available on request.

## References

[1] M.C. Lemme, S. Wagner, K. Lee, X. Fan, G.J. Verbiest, S. Wittmann, S. Lukas, R.J. Dolleman, F. Niklaus, H.S. van der Zant, et al., Nanoelectromechanical sensors based on suspended 2D materials, Research 2020 (2020).
[2] D. Hälg, T. Gisler, Y. Tsaturyan, L. Catalini, U. Grob, M.-D. Krass, M. Héritier, H. Mattiat, A.-K. Thamm, R. Schirhagl, et al., Membrane-based scanning force microscopy, Phys. Rev. Appl. 15 (2) (2021) L021001.
[3] B.R. Samanta, F. Pardo, T. Salamon, R. Kopf, M.S. Eggleston, Low-cost electrothermally actuated MEMS mirrors for high-speed linear raster scanning, Optica 9 (2) (2022) 251–257.
[4] T. Cao, T. Hu, Y. Zhao, Research status and development trend of MEMS switches: A review, Micromachines 11 (7) (2020) 694.
[5] X.C. Tong, Advanced Materials and Components for 5G and Beyond, Springer, 2022.
[6] G. Brawley, M. Vanner, P.E. Larsen, S. Schmid, A. Boisen, W. Bowen, Nonlinear optomechanical measurement of mechanical motion, Nature Commun. 7 (1) (2016) 10988.
[7] A. Bachtold, J. Moser, M. Dykman, Mesoscopic physics of nanomechanical systems, Rev. Modern Phys. 94 (4) (2022) 045005.
[8] F. Yang, M. Fu, B. Bosnjak, R.H. Blick, Y. Jiang, E. Scheer, Mechanically modulated sideband and squeezing effects of membrane resonators, Phys. Rev. Lett. 127 (18) (2021) 184301.
[9] D. Shin, A. Cupertino, M.H. de Jong, P.G. Steeneken, M.A. Bessa, R.A. Norte, Spiderweb nanomechanical resonators via bayesian optimization: inspired by nature and guided by machine learning, Adv. Mater. 34 (3) (2022) 2106248.
[10] T.M. Karg, B. Gouraud, C.T. Ngai, G.-L. Schmid, K. Hammerer, P. Treutlein, Light-mediated strong coupling between a mechanical oscillator and atomic spins 1 meter apart, Science 369 (6500) (2020) 174–179.
[11] E.P. Tomasini, P. Castellini, Laser Doppler Vibrometry, Springer, 2020.
[12] L. Scislo, Single-point and surface quality assessment algorithm in continuous production with the use of 3D laser doppler scanning vibrometry system, Sensors 23 (3) (2023) 1263.
[13] S. Petitgrand, R. Yahiaoui, K. Danaie, A. Bosseboeuf, J. Gilles, 3D measurement of micromechanical devices vibration mode shapes with a stroboscopic interferometric microscope, Opt. Lasers Eng. 36 (2) (2001) 77–101.
[14] R. Waitz, C. Lutz, S. Nößner, M. Hertkorn, E. Scheer, Spatially resolved measurement of the stress tensor in thin membranes using bending waves, Phys. Rev. Appl. 3 (4) (2015) 044002.
[15] F. Yang, F. Rochau, J.S. Huber, A. Brieussel, G. Rastelli, E.M. Weig, E. Scheer, Spatial modulation of nonlinear flexural vibrations of membrane resonators, Phys. Rev. Lett. 122 (15) (2019) 154301.
[16] D. Hoch, K.-J. Haas, L. Moller, T. Sommer, P. Soubelet, J.J. Finley, M. Poot, Efficient optomechanical mode-shape mapping of micromechanical devices, Micromachines 12 (8) (2021) http://dx.doi.org/10.3390/mi12080880.
[17] A. Moreau, D. Borza, I. Nistea, Full-field vibration measurement by time-average speckle interferometry and by Doppler vibrometry–A comparison, Strain 44 (5) (2008) 386–397.
[18] F. Yang, M. Fu, R. Waitz, E. Scheer, Quantitative signal extraction in the dynamic range of nanomechanical systems by free and constrained fitting, Sensors Actuator A 354 (2023) 114307.
[19] R. Waitz, S. Nößner, M. Hertkorn, O. Schecker, E. Scheer, Mode shape and dispersion relation of bending waves in thin silicon membranes, Phys. Rev. B 85 (3) (2012) 035324.
[20] M. Fu, B. Bošnjak, Z. Shi, J. Dornseiff, R.H. Blick, E. Scheer, F. Yang, A hybrid graphene-siliconnitride nanomembrane as a versatile and ultra-widely tunable mechanical device, 2024, arXiv preprint arXiv:2406.11596.
[21] P. Jourdain, D. Boss, B. Rappaz, C. Moratal, M.-C. Hernandez, C. Depeursinge, P.J. Magistretti, P. Marquet, Simultaneous optical recording in multiple cells by digital holographic microscopy of chloride current associated to activation of the ligand-gated chloride channel GABAA receptor, PLoS One 7 (12) (2012) e51041.
[22] A. Keşkekler, O. Shoshani, M. Lee, H.S. van der Zant, P.G. Steeneken, F. Alijani, Tuning nonlinear damping in graphene nanoresonators by parametric–direct internal resonance, Nature Commun. 12 (1) (2021) 1099.
[23] F. Yang, F. Hellbach, F. Rochau, W. Belzig, E.M. Weig, G. Rastelli, E. Scheer, Persistent response in an ultrastrongly driven mechanical membrane resonator, Phys. Rev. Lett. 127 (1) (2021) 014304.
[24] M. Fu, O. Ameye, F. Yang, J. Košata, J. del Pino, O. Zilberberg, E. Scheer, Fluctuation instabilities via internal resonance in a multimode membrane as a mechanism for frequency combs, 2024, arXiv preprint arXiv:2409.15138.
[25] Y. Patil, S. Chakram, L. Chang, M. Vengalattore, Thermomechanical two-mode squeezing in an ultrahigh-Q membrane resonator, Phys. Rev. Lett. 115 (1) (2015) 017202.
[26] A. Ganesan, C. Do, A. Seshia, Phononic frequency comb via intrinsic three-wave mixing, Phys. Rev. Lett. 118 (3) (2017) 033903.

**Dr. Mengqi Fu** graduated as Dr. rer. nat. at Peking University (China) in 2016. She worked as researcher in the department of microwave engineering at Shanghai Academy of Spaceflight Technology (China) from 2016 to 2017 and as patent engineer in Liu Shen & Associate (China) from 2017 to 2018. Since 2018, she works as postdoctoral fellow in the department of physics at University of Konstanz (Germany).

**M.Sc. Jannik Dornseiff** obtained his B.Sc. in Physics in 2018 and his M.Sc. in Physics in 2021 from the University of Konstanz, Germany. He has been a Ph.D. candidate at the University of Konstanz since 2021.

**M.Sc. Valentin Barth** obtained his B.Sc. in Physics in 2021 and his M.Sc. in Physics in 2023 from the University of Konstanz, Germany. He has been a Ph.D. candidate at the University of Konstanz since 2023.

**Prof. Dr. Elke Scheer** graduated as Dr. rer. nat. at the University of Karlsruhe (Now: Karlsruhe Institute of Technology, KIT) in Germany in 1995. She worked as postdoctoral fellow at the Quantronics Group at Commissariat à l'Energie Atomique Saclay, France, from 1996 to 1997 and as Assistant Professor (C1) at KIT from 1997-2000. Since 2000 she is professor of experimental physics at the University of Konstanz, Germany.